Available online at www.sciencedirect.com
SCIENCE DIRECT
Journal of Magnetic Resonance 181 (2006) 1–8
JMR Journal of Magnetic Resonance
www.elsevier.com/locate/jmr

Recoupling of chemical-shift anisotropy powder patterns in MAS NMR

Robin M. Orr, Melinda J. Duer *

Department of Chemistry, University of Cambridge, Lensfield Road, Cambridge CB2 1EW, UK

Received 31 January 2006; revised 10 March 2006
Available online 30 March 2006

Abstract

A comparison of three different implementations of the chemical-shift recoupling experiment of Tycko et al. [R. Tycko, G. Dabbagh, P.A. Mirau, Determination of chemical-shift-anisotropy lineshapes in a two-dimensional magic-angle-spinning NMR experiment, J. Magn. Reson. 85 (1989) 265–274] is presented. The methods seek to reduce the effects of artefacts resulting from pulse imperfections and residual C-H dipolar coupling in organic solids. An optimised and constant time implementation are shown to give well-defined and artefact free powder pattern lineshapes in the indirectly observed dimension for both sp^2 and sp^3 carbon sites. Experimental setup is no more demanding than for the original experiment, and can be implemented using standard commercial hardware.

Keywords: Solid-state NMR; Magic-angle spinning; Chemical-shift anisotropy; Recoupling

1. Introduction

Chemical-shift anisotropy (CSA) measurements have found numerous applications in solid-state NMR for obtaining structural and motional information by the simple analysis of static (or quasi-static) lineshapes and spinning sideband intensities [1–5]. Additional information is often gained from more complex experiments that further modulate the CSA powder pattern or spinning sideband intensities according to other interactions, such as relative orientation of CSA and dipolar tensors [6–8], allowing a variety of different structural features to be investigated. Detailed discussion of the relative merits of using CSA powder patterns compared with spinning sideband measurements has been reported elsewhere [9,10] and we reiterate only the main points that powder patterns allow immediate recognition of molecular motion, existence of partial orientation, and accurate determination of the chemical-shift asymmetry parameter, whilst spinning sideband intensity analysis enjoys higher sensitivity and may permit higher accuracy in the determined chemical-shift anisotropy parameter.

For samples that contain a number of different nuclear environments, it is most common to follow the approach introduced by Alla et al. [11], whereby MAS is used to record a high-resolution spectrum in the directly observed dimension of a two-dimensional (2D) experiment, while recoupling the CSA in the indirect dimension. Methods that give either spinning sideband intensities [4,12–18] or quasi-static powder patterns [10,19–24] have been reported. A brief review of many of these methods was made by Liu et al. [10]. Of interest in this work are methods to recouple static powder patterns that can be implemented using standard commercial hardware, available in most NMR laboratories, and so methods such as magic-angle turning [25,19,20] or variable-angle correlation spectroscopy [26] experiments, whilst very effective in many cases, are not discussed here.

One particularly elegant and simple method to recouple quasi-static CSA powder patterns is the experiment of Tycko and co-workers [21], which involves applying 4 or 6 π-pulses per rotor period; for convenience we refer to this experiment as '2DCSA.' Unfortunately, in practice it suffers from a high sensitivity to residual C-H dipolar

* Corresponding author. Fax: +44 1223 336362.
E-mail address: mjd13@cam.ac.uk (M.J. Duer).

1090-7807/$ - see front matter © 2006 Elsevier Inc. All rights reserved.
doi:10.1016/j.jmr.2006.03.010

coupling [27] and pulse imperfections, and in addition it cannot be used at high spinning frequencies as finite pulse length effects introduce additional artefacts [21]. Modifications of the original experiment have been reported: in a recent study, Witter et al. [28] demonstrated that higher spinning frequencies (~10 kHz) could be used if the π-pulses were applied over three rotor periods rather than one. In addition, a major development was made by Liu et al. [10] in presenting the SUPER experiment that replaces the π-pulses with 2π-pulses, in a similar manner to the method of Bax et al. [18], and consequently reduces the effects of residual C-H dipolar coupling. Moreover, using SUPER, the demands on the probe in terms of pulse field strength requirements is reduced.

The modifications of 2DCSA that we present here also aim to reduce the effects of residual C-H dipolar coupling and of pulse imperfections on the CSA recoupling spectra obtained, but keep the original form of the experiment that is simple and convenient to set up. Three different implementations have been considered in this work to minimise these problems and produce the best possible quality lineshapes in F_1. First, introducing cogwheel phase cycling minimises the effects of pulse imperfection on the spectra recorded; second, a constant time version of the experiment removes the effects of residual C-H dipolar coupling; and finally, a method that minimises the number of pulses used during t_1 evolution is described, which optimises the signal-to-noise ratio.

2. Theory and methods

The 2DCSA pulse sequence is reproduced in Fig. 1. In general $(2n+2)$ π-pulses (for integer n) are applied symmetrically about the centre of an odd number (m) of rotor periods (τ_r); this forms one 'pulse-sequence unit.' The t_1 evolution period is incremented during the 2D experiment by increasing the number of pulse-sequence units (j). For each crystallite in the sample, the effect of the pulse sequence is to recouple the chemical-shift interaction such that the evolution that results during t_1 is equivalent to that which would occur if the crystallite had remained in its initial orientation at the start of the pulse sequence instead of being rotated by MAS, except that the isotropic and anisotropic components of the chemical-shift interaction are scaled by the factors ξ and χ, respectively [21]. These scaling factors are given by:

$$\chi = \frac{2}{m\tau_r}\int_0^{m\tau_r/2} f(t)\cos(\Omega_r t)\mathrm{d}t \quad \xi = \frac{2}{m\tau_r}\int_0^{m\tau_r/2} f(t)\mathrm{d}t, \qquad (1)$$

where $f(t)$ is a step function that is equal to 1 at times $t = \pm m\tau_r/2$ and changes sign at the centre of each π-pulse, according to the time coordinate shown in Fig. 1.

For a crystallite with orientation $\Omega(\alpha,\beta,\gamma)$ with respect to the rotor frame at the end of the cross-polarisation spin-lock pulse, the total phase evolution during a t_1 period in which j pulse-sequence units are applied is:

$$\phi(\Omega) = (\xi\delta + \chi[C_1(\Omega) + C_2(\Omega)])jm\tau_r, \qquad (2)$$

where $C_1(\Omega)$ and $C_2(\Omega)$ describe the dependence of the anisotropic part of the chemical shift on the crystallite orientation and are described in detail by Maricq and Waugh [31].

Using four π-pulses over one rotor period, there are pulse times available that give anisotropic scaling factors over the continuous range $\chi = 0\ldots0.412$, with a corresponding non-zero isotropic scaling factor, except for $\chi = 0.393$. If six π-pulses are applied over an odd number of rotor periods then pulse times are available for a continuous range of anisotropic scaling factors with the isotropic scaling factor equal to zero. This latter point can be used to avoid aliasing of powder patterns when a large range of isotropic chemical shifts are present. Over one rotor period, the anisotropic scaling factor varies in the range $\chi = -0.4\ldots0.395$, and over three rotor periods, $\chi = -0.242\ldots0.13$ with $\xi = 0$ in both cases.

As noted previously, the effects of finite pulse lengths, B_1 field inhomogeneity and incorrect pulse calibration lead to artefacts appearing in the spectrum. These are found largely near the edge of the F_1 dimension of the spectra if an appropriate alternation of the phases of the π-pulses in the pulse sequence is used [21]. This prevents the use of the sequences that would lead to aliasing as, after shearing, the spectrum would contain the artefacts within the powder patterns. More importantly, it is often found that highly broadened lineshapes are recorded for the powder patterns compared with powder patterns recorded under static condition. This additional line broadening corresponds to rapid decay of the signal intensity during t_1 evolution, and results from the loss of signal following the desired phase evolution because of additional evolution under residual C-H dipolar coupling during the application of π-pulses and from pulse imperfections, as the number of pulses applied during the t_1 evolution is increased.

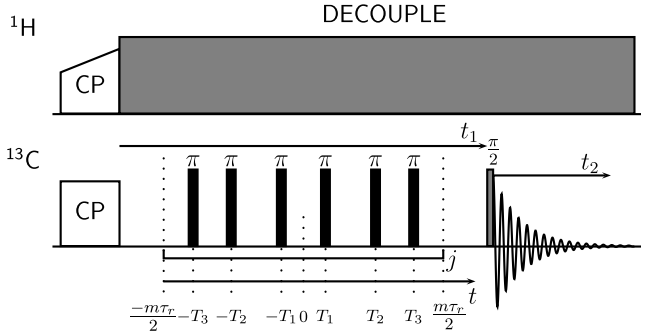

Fig. 1. 2DCSA pulse sequence. In this example, six π-pulses are applied over m rotor periods. During the t_1 evolution period the six π-pulse unit is applied j times, followed by a π/2-pulse that is used to record sine and cosine amplitude-modulated signals to achieve absorption mode lineshapes [29,30].

2.1. Cogwheel phase cycling

Cogwheel phase cycling can often reduce the number of phase cycle steps required in an experiment. In particular,

when only π-pulses are applied during the experiment, the reduction is dramatic; as Levitt and co-workers commented [32], for p π-pulses, a minimum of $2p+1$ phase cycle steps are required to select only the $\{+1 \rightarrow -1 \rightarrow +1 \rightarrow -1 \rightarrow +1 \rightarrow -1 \rightarrow \ldots\}$ coherence pathway, although using a greater number of steps in the cycle does not alter the selectivity of the phase cycle in this specific case. If we consider the example of using the six π-pulse sequence and collecting 32 points in the t_1 dimension, this would require nearly 400 phase cycle steps (using cogwheel phase cycling) to select for the unique coherence pathway for all slices in the t_1 dimension; whilst this requires a relatively large number of scans per slice in the t_1 dimension, it may be feasible for many samples and, moreover, may be necessary for samples with a low sensitivity. A similar cogwheel phase cycling scheme could also be implemented for the SUPER experiment [10], although we have not investigated this.

Cogwheel phase cycling becomes much more difficult to implement when pulses other that π-pulses are used, but amplitude-modulated signals cannot be recorded when only π-pulses are applied during the pulse sequence. Instead, we record two phase-modulated signals according to the echo–antiecho method of phase-sensitive detection [30,33]. This is achieved, as suggested by Bachmann and co-workers [33], by using a π-pulse just prior to acquisition (rather than a π/2 pulse as is usually used in the States method of detection [29]) to record one dataset, and in a second experiment this π-pulse is omitted. One of the two dataset will correspond to the echo (p-type) signal and the other the antiecho (n-type) signal. In the following sections, we refer to this implementation as 2DCSA(COG). A point of concern may be raised: the echo and antiecho signals will not be recorded with equal efficiency due to imperfections in the additional π-pulse used in detecting one of these signals, and so true double absorption lineshapes in the 2D spectrum cannot be achieved. However, in practice, we have not observed significant distortions of the lineshape in either dimension of the spectrum using the echo–antiecho method. Furthermore, the alternative is to use the conventional phase scheme with the States method of detection, where pulse imperfections result in potentially large glitches at the edge of the spectrum and distorted lineshapes.

2.2. Constant time implementation

As expressed in Eq. (2), the phase evolution during the t_1 period may be incremented by increasing the number of pulse units (increasing j); this is the method that is conventionally used. If the isotropic scaling factor is chosen to be zero (and hence 6 π-pulses per pulse-sequence unit are used), then the phase evolution during the t_1 period may instead be incremented by changing either j or the anisotropic scaling factor χ, which simply involves changing the pulse times used in the sequence. Alternatively both j and χ can be varied during the experiment.

If j is kept constant and equal to j_{total}, then the experiment becomes a constant time experiment (CT-2DCSA). This has the advantage that the effect of residual dipolar coupling during the application of π-pulses is removed. The obvious penalty is that the signal-to-noise of the recorded spectrum may be significantly reduced because of the relatively large number of π-pulses involved. The spectral width (SW) in the indirect dimension and the anisotropic scaling factor $\chi(k)$ of the kth t_1 slice in the experiment are related by:

$$\frac{k-1}{SW} = \frac{m j_{\text{total}} \chi(k)}{\nu_{\text{r}}} \quad 1 \leqslant k \leqslant k_{\max}, \tag{3}$$

where ν_{r} is the spinning frequency, m is the number of rotor periods in the pulse-sequence unit, j_{total} is the number of pulse-sequence units used, and $k_{\max}$ is the total number of points recorded in the t_1 dimension. The required value of j_{total} is calculated from:

$$j_{\text{total}} = \text{Ceil}\left(\frac{\nu_{\text{r}}(k_{\max}-1)}{SW \chi_{\max} m}\right), \tag{4}$$

where $\text{Ceil}(x)$ rounds up x to the nearest integer and $\chi_{\max}$ is the largest value of χ possible in the allowable range of χ scaling factors with $\xi = 0$. From Eq. (4), the greater the value of $\chi_{\max} m$, the smaller j_{total} (total number of pulse-sequence units) and hence the smaller the number of π-pulses required in the sequence. For this reason, it is advantageous to use the pulse-sequence unit over three rotor periods ($m = 3$, $\chi_{\max} = 0.242$) rather than that lasting one rotor period ($m = 1$, $\chi_{\max} = 0.395$).

The anisotropic scaling factor required for each point k in the t_1 dimension can then be calculated according to:

$$\chi(k) = \frac{\nu_{\text{r}}/mSW(k-1)}{\text{Ceil}\left(\frac{\nu_{\text{r}}(k_{\max}-1)}{SW \chi_{\max} m}\right)}. \tag{5}$$

For a typical powder pattern, recorded such that the powder pattern covers the majority of the spectral width, collecting 32 points will often be sufficient to define the powder pattern. To obtain undistorted, static-like powder patterns and to optimise the signal-to-noise ratio, the experimental conditions should be constrained to spinning frequencies sufficiently large that only low order spinning sidebands in the direct dimension are obtained. For these purposes, it is sufficient to use spinning frequencies greater than half the chemical-shift anisotropy of the powder pattern being measured.

Fig. 2 illustrates the dependence of j_{total} on SW/ν_{r}, for recording 32 points in the t_1 period ($m = 3$, $\chi_{\max} = 0.242$). There is a relatively narrow, but useful, practical range with $SW/\nu_{\text{r}} \approx 6$, that corresponds to using between six and ten pulse-sequence units. In a 9.4 T magnetic field and for sp^2 carbon nuclei, spinning frequencies around 5 kHz are sufficient to provide a suitable spectral width in F_1 whilst not having too great a sideband intensity in F_2, and for sp^3 sites slower spinning, ~2.5 kHz, will be preferable. At higher fields, faster spinning could be

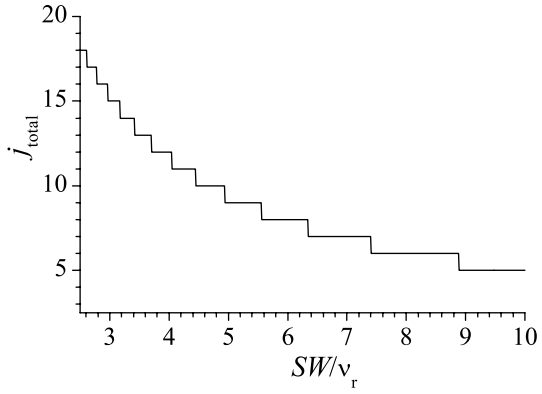

Fig. 2. Variation of the total number of pulse-sequence units required, j_{total}, with the SW/ν_r ratio.

implemented since the six pulses are applied over three rotor periods [28].

2.3. Optimised implementation

An alternative approach is to optimise the experiment such that the minimum number of π-pulses is used for each slice of the t_1 dimension (OPT-2DCSA). This should give the best possible signal-to-noise ratio. Accordingly, the number of pulse units, and anisotropic scaling factor, required for the kth increment of the t_1 period are:

$$j(k) = \mathrm{Ceil}\left(\frac{\nu_r(k-1)}{SW\chi_{max}m}\right) \quad 1 \leqslant k \leqslant k_{max}, \tag{6}$$

$$\chi(k) = \frac{\nu_r/mSW(k-1)}{\mathrm{Ceil}\left(\frac{\nu_r(k-1)}{SW\chi_{max}m}\right)} \quad 1 \leqslant k \leqslant k_{max}. \tag{7}$$

This will minimise the signal decay due to the effect of the imperfect pulses, and thus benefit from a greater signal-to-noise ratio than for the constant time experiment. There will, however, be some effect from residual C-H dipolar coupling. The maximum number of pulse-sequence units, which occurs for the last t_1 slice of the experiment, is the same j_{total} for the constant time experiment with the same spectral width and spinning frequency.

Increasing the number of pulse-sequence units applied during the t_1 evolution in a nonlinear manner will cause a non-exponential ('stepped-exponential') decay of the t_1 signal (as a result of pulse imperfections), and for individual crystallites non-Lorentzian lineshapes in the frequency domain will result. To illustrate this effect, in Fig. 3 we show three different decay functions, each of the form $\exp\{-j(k)m\tau_r/T_{decay}\}$, where T_{decay} is the same for all decays functions shown and $j(k)$ (defined in Eq. (6)) is different in each case. The Fourier transforms of the stepped-exponential functions yield much sharper lines, as expected. However, there are slight artefacts in the baseline for these functions. Since the experimental spectra correspond to the true powder pattern convoluted with the Fourier transform of the stepped-exponential function, the OPT-2DCSA method could introduce new artefacts into

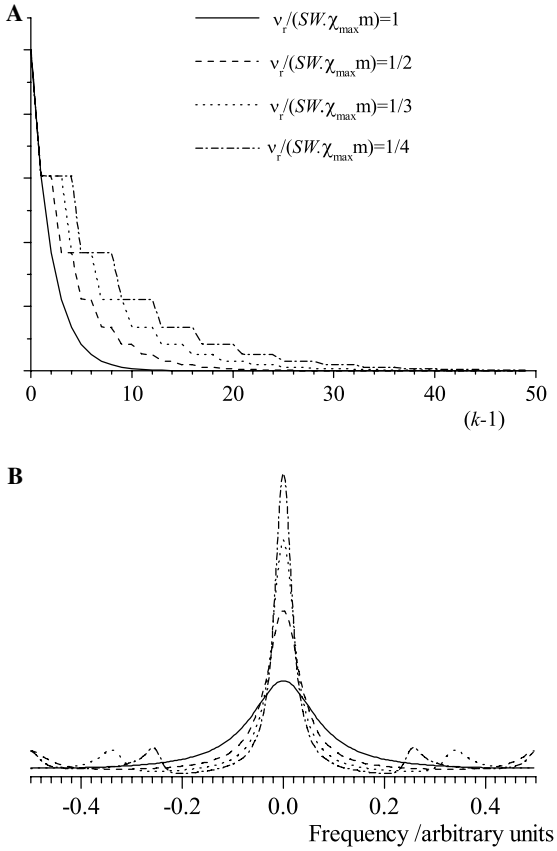

Fig. 3. (A) Stepped-exponential decay functions $\exp\{-j(k)m\tau_r/T_{decay}\}$, where T_{decay} is a time constant that describes the signal attenuation with increasing pulse-sequence units and $j(k) = \mathrm{Ceil}(\nu_r(k-1)/(SW\chi_{max}m))$. Four values of $\nu_r/(SW\chi_{max}m)$ are illustrated. (B) The corresponding Fourier transforms of the functions in (A).

the spectrum. However, these artefacts will be small, except in cases of rapid signal decay due to imperfect pulses, in which case it is unlikely that useful results will be obtained by multiple π-pulse recoupling experiments in any case.

In both the CT-2DCSA and OPT-2DCSA implementations, we use cogwheel phase cycling. Stable spinning is clearly essential in all three cases. Standard commercial hardware routinely stabilises spinning to ±2 Hz, which we have found sufficient, although other stable spinning systems have been reported that achieve higher precision [34].

3. Experimental

All experiments were implemented using a Bruker Avance spectrometer operating at 100.56 MHz for ^{13}C and 399.98 MHz for ^{1}H, using a 4 mm zirconia rotor and standard spinning hardware that stabilised spinning to within ±2 Hz. TPPM [35] or SPINAL-64 [36] ^{1}H decoupling was used with a field strength of ~100 kHz, ^{13}C field strengths for the π-pulses were ~80 kHz and cross-polarisation [37] was used with a ramped spin-lock pulse [38] applied to the ^{1}H channel. All samples were obtained from Sigma–Aldrich and used without further purification and

the rotors were packed *without* restricting the volume to the centre of the rotor.

To implement the pulse sequences, we use a simple procedure written using MuPAD [39] to calculate the required anisotropic scaling factor for each point sampled in the t_1 dimension. The pulse times to be used for each t_1 increment of the experiment are determined by substituting in the required anisotropic scaling factor and solving the two nonlinear Eqs. (8) and (9), together with Eq. (10) (which are derived from reference [21]):

$$\sin\left(\frac{2\pi(T_2-T_1)}{\tau_r}+\frac{\pi m}{2}\right)+\sin\left(\frac{2\pi T_1}{\tau_r}\right)-\sin\left(\frac{2\pi T_2}{\tau_r}\right)-\frac{\pi\chi(k)n}{2}=0, \quad (8)$$

$$\sin\left(\frac{4\pi(T_2-T_1)}{\tau_r}+\pi m\right)+\sin\left(\frac{4\pi T_1}{\tau_r}\right)-\sin\left(\frac{4\pi T_2}{\tau_r}\right)-\pi\chi(k)n=0, \quad (9)$$

$$T_3=T_2-T_1+m\tau_r/4, \quad (10)$$

where T_1, T_2, and T_3 are defined in Fig. 1. These procedures are available on request.

The pulse times and number of pulse-sequence units for each t_1 point were written to files that were read by the pulse program, so that storing several different versions of the pulse program were not required. Alternatively, the pulse times could be parametrised with respect to the anisotropic scaling factor, to allow the pulse times to be calculated automatically at run time by the pulse program.

Cogwheel phase cycling employed winding numbers of 0 and 1 for alternate pulses in the sequence, ensuring that the last pulse in the sequence has a winding number of 1. In addition the ^{1}H excitation pulse was alternated in phase between 0 and π on consecutive acquisitions and the receiver phase adjusted appropriately.

Between 100 and 400 scans were recorded per t_1 increment of the experiment, with the experiments lasting between 6 and 20 h.

Numerical simulations of powder patterns were performed using the SIMPSON simulation package [40]. The simulations shown in Figs. 4–6 used 32 points and zero filling to 256 points; no apodisation of the FID was used.

4. Results and discussion

As an initial demonstration of the three implementations of 2DCSA, a comparison of the spectra obtained by each method was made using ^{13}C-1-glycine, and Fig. 4 shows slices from the F_1 dimension of the spectrum for the carbonyl site. The correct form of powder pattern was obtained using each method, confirming that they can all be implemented in practice.

Comparing Figs. 4(a) and (b), the cogwheel phase cycle clearly suppresses the major artefacts seen at the edge of the spectrum seen in Fig. 4(a). Another useful application of this type of cogwheel phase cycling may be in REAPDOR experiments [41], in which several π-pulses must be applied to observed nucleus and pulse imperfections can

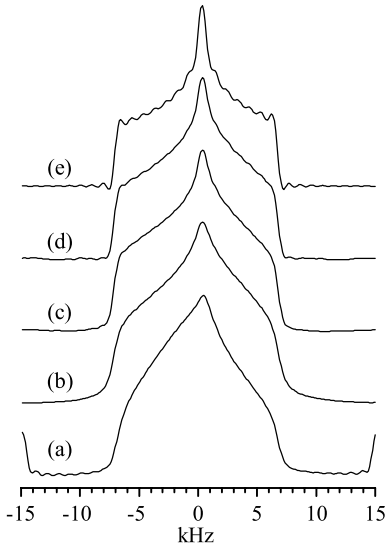

Fig. 4. F_1 slices of the carbonyl site of glycine extracted for the 2D spectra for (a) the conventional implementation of the 2DCSA experiment, (b) the 2DCSA(COG) implementation, (c) the OPT-2DCSA(COG) implementation, (d) the CT-2DCSA(COG) implementation, and (e) a simulated powder pattern, based on static powder pattern measurements of the CSA parameters $\Delta_{CS}=-71$ ppm, $\eta_{CS}=0.91$. In all cases, $\nu_r=5000$ Hz and $SW=30$ kHz, and for (c) and (d) $j_{total}=8$.

lead to deviation from the expected signal decay. The CT-2DCSA(COG) and OPT-2DCSA(COG) methods give improved sharpness at the discontinuities in the powder pattern together with improved lineshapes. For the 2DCSA(COG) experiment shown, the complete phase cycle of 378 steps was used. This selects only the desired coherence pathway for all 32 slices of the t_1 dimension; in practice we have found that the number of steps in the phase cycle can be reduced by a factor of two without introducing obvious artefacts into the spectrum. Analysis of the cogwheel selection diagram [32,42] shows that this reduction of the number of steps in the phase cycle will select unwanted phase signatures in addition to the desired coherence pathway. For a complete phase cycle of N steps, reducing the cycle to $N/2+1$ steps will result in a phase cycle that still selects only the desired coherence pathway for the first half of the slices in the t_1 dimension, and one unwanted phase signature for the second half of the t_1 slices recorded. Since the first few t_1 points are most important for defining the powder pattern, and the unwanted phase signature selected for the remaining slices represents a relatively small fraction of the total unwanted coherence pathways, using the reduced phase cycle does not appear to affect the recorded spectra.

Fumaric acid monoethyl ester is a useful sample on which to test these modifications of 2DCSA, as it contains a variety of sp^2 and sp^3 hybridised carbon sites. In this case, we compare the results for the 2DCSA(COG), OPT-2DCSA(COG), and CT-2DCSA(COG) implementations (Fig. 5). For all the sites, there is a noticeable advantage in using the modified versions of the experiment, with an excellent correspondence between the simulated and

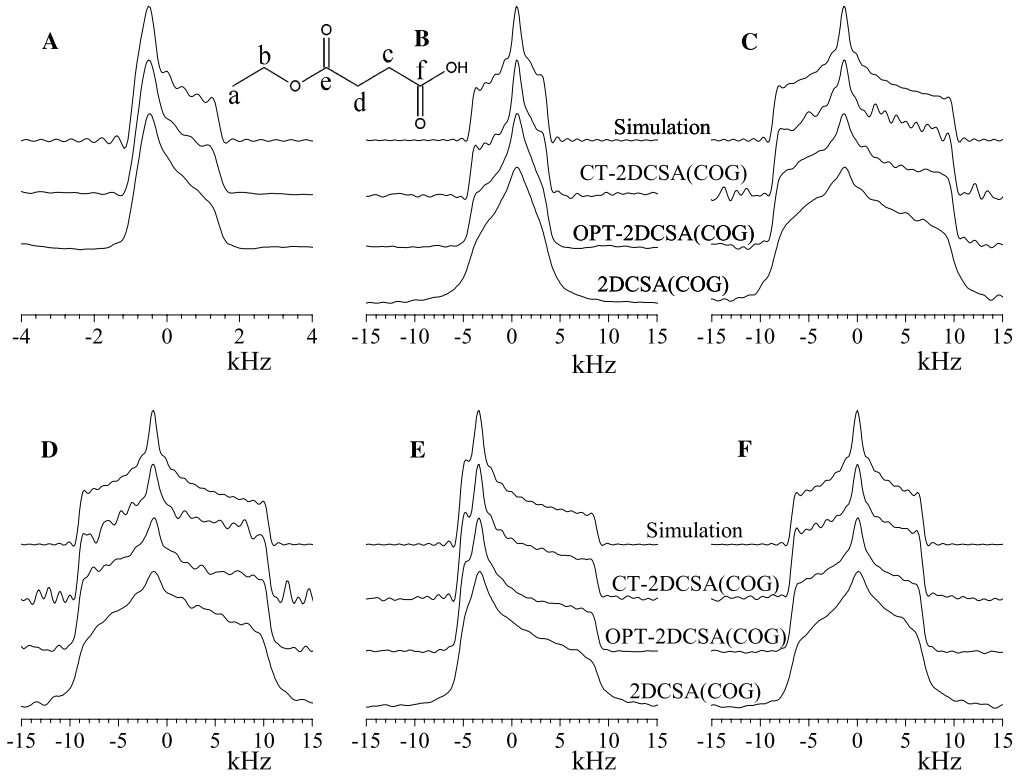

Fig. 5. F_1 slices of the six carbon sites of fumaric acid for the 2DCSA(COG), OPT-2DCSA(COG), CT-2DCSA(COG) implementations, and corresponding simulated powder pattern. For site (A) the spinning frequency used was 2350 Hz with a spectral width of 13 kHz in the indirectly detected dimension. For sites (B–F) the spinning frequency used was 5750 Hz with a spectral width of 32 kHz. In both cases, $j_{\text{total}} = 8$ for the constant time method. For the 2DCSA(COG) results a 206 step phase cycle was used, selecting at most only one unwanted phase signature.

CT-2DCSA results for each carbon environment with CSA parameters consistent with values determined using an alternative experiment [16]. The slight deviation away from simulated 'ideal' pattern arises because the contribution to the centreband in the directly observed dimension is not the same for all crystallites; nevertheless, the discontinuities of the lineshape remain in the same position.

The improvement on using the optimised versions is especially noticeable in Fig. 5(B), which is a CH_2 site and so suffers particularly seriously from the effects of C-H dipolar coupling. Apodisation was not used for any of the spectra shown, and so some small truncation artefacts can be seen in some of the results, although these do not obscure the discontinuities in the powder patterns.

A lower signal-to-noise ratio is evident for the constant time implementation; despite this, very well-defined powder patterns are obtained. This implementation may find useful application for separating overlapping powder patterns with the same isotropic shift where excellent resolution of the powder pattern is needed if the component

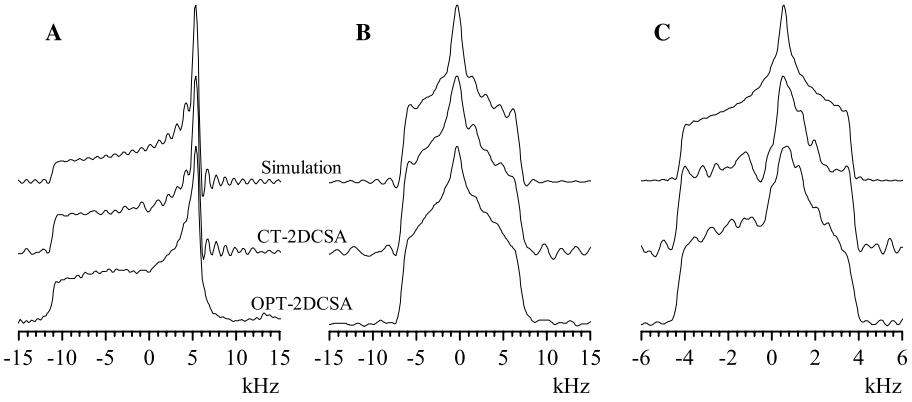

Fig. 6. Experimental results for (A) the sp^2 site in hexamethyl benzene and simulated powder pattern using $\Delta_{CS} = -111$ ppm, $\eta = 0$ [43]. (B) The carbonyl carbon of histidine monohydrochloride monohydrate $\Delta_{CS} = 68$ ppm, $\eta = 0.90$, recorded at a spinning frequency of 5750 Hz, $SW = 32$ kHz, and $j_{\text{total}} = 8$. (C) The CH_2 carbon of fumaric acid monoethyl ester recorded with $\nu_r = 2350$ Hz, $SW = 13$ kHz, and $j_{\text{total}} = 8$.

powder patterns are to be unambiguously simulated. There are no obvious artefacts present in the results obtained using the OPT-2DCSA(COG) version, and the powder patterns compare favourably with those obtained using 2DCSA(COG), suggesting that this is a useful compromise when the signal-to-noise ratio using the constant time implementation is insufficient.

When the asymmetry parameter is small, then collecting 32 points during the t_1 evolution may be insufficient, as extensive truncation artefacts will be seen in the spectrum unless apodisation of the data is performed using an appropriate function, which would negate the benefits of this implementation. For example, we show the spectrum for the sp^2 carbon of hexamethyl benzene in Fig. 6(A), in which the chemical shielding asymmetry parameter is zero [43]. Collecting many more than 32 points using the CT-2DCSA(COG) version of the experiment becomes difficult to implement as it requires an excessively long pulse train; in this case, the better choice may be the OPT-2DCSA (COG) implementation. The powder pattern recorded using OPT-2DCSA(COG) is also shown in Fig. 6(A), where 50 points were collected during the t_1 evolution and sinc oscillations are no longer seen. Two further examples of results obtained for the carbonyl site of L-histidine monohydrochloride monohydrate, and the CH_2 site of fumaric acid monoethyl ester recorded using a smaller spectral width than in Fig. 5 are also shown in Fig. 6 to illustrate typical results.

5. Conclusion

Cogwheel phase-cycled, constant time, and optimised implementations of the CSA recoupling experiment of Tycko and co-workers [21] have been investigated. It has been demonstrated that the modifications give reliable, undistorted chemical-shift anisotropy powder patterns using a standard experimental hardware and methods. The constant time (CT-2DCSA(COG)) variant was shown to give the optimum lineshapes for the powder patterns, while the optimised (OPT-2DCSA(COG)) version of the experiment maximised the signal-to-noise ratio. Experimentally, the methods are no more complicated, or time consuming, to set up than the original version of the CSA recoupling experiment proposed by Tycko [21] and may prove useful for laboratories that do not posses slow spinning or variable-angle spinning hardware. In addition, for the purposes of quantitative evaluation of the chemical-shift principal values, the lineshapes obtained by these modifications compare favourably with those from other methods.

Acknowledgments

R.M.O. is grateful to the Engineering and Physical Sciences Research Council (EPSRC) for a studentship. This work was performed as part of an EPSRC-funded project, GR/R96897.

References

[1] W.S. Veeman, Carbon-13 chemical shift anisotropy, Prog. Nucl. Magn. Reson. 16 (1984) 193–235.
[2] H.W. Spiess, Molecular motion studied by NMR powder spectra. i. lineshape calculation for axially symmetric shielding tensors, Chem. Phys. 6 (1974) 217–225.
[3] M.S. Solum, K.W. Zilm, J. Michl, D.M. Grant, Carbon-13 line shape study of two-site exchange in solid dimethyl sulfone, J. Phys. Chem. 87 (1983) 2940–2944.
[4] O.N. Antzutkin, Y.K. Lee, M.H. Levitt, ^{13}C and ^{15}N chemical shift anisotropy of ampicillin and penicillin-v studied by 2D-PASS and CP/MAS NMR, J. Magn. Reson. 135 (1998) 144–155.
[5] M.J. Duer, M.H. Levitt, Time-domain calculation of chemical exchange effect in the NMR spectra of rotating solids, Solid State Nucl. Magn. Reson. 1 (1992) 211–215.
[6] P. Palmas, C. Malveau, P. Tekely, D. Canet, Magnitudes and mutual orientation of dipolar and shielding interaction tensors determined from the orientation dependence of spinning sidebands of slowly rotating powder samples, Solid State Nucl. Magn. Reson. 13 (1998) 45–53.
[7] M. Strohmeier, D.W. Alderman, D.M. Grant, Obtaining molecular and structural information from ^{13}C–^{14}N system with ^{13}C FIREMAT experiments, J. Magn. Reson. 155 (2002) 263–277.
[8] X. Yao, M. Hong, Determination of Cα chemical shift tensor orientation in peptides by dipolar-modulated chemical shift recoupling NMR spectroscopy, J. Am. Chem. Soc. 124 (2002) 2730–2738.
[9] P. Hodgkinson, L. Emsley, The reliability of the determination of tensor parameters by solid-state nuclear magnetic resonance, J. Chem. Phys. 107 (1997) 4808–4816.
[10] S. Liu, J. Mao, K. Schmidt-Rohr, A robust technique for two-dimensional separation of undistorted chemical-shift anisotropy powder patterns in magic-angle-spinning NMR, J. Magn. Reson. 155 (2002) 15–28.
[11] M.A. Alla, E.I. Kundla, E.T. Lippmaa, Selective determination of anisotropic magnetic interactions from high-resolution NMR spectra of powdered samples, JETP Lett. 27 (1978) 194–197.
[12] C. Crockford, H. Geen, J.J. Titman, Two-dimensional MAS-NMR spectra which correlate fast and slow magic-angle spinning sideband patterns, Chem. Phys. Lett. 344 (2001) 367–373.
[13] B. Eléna, S. Hediger, L. Emsley, Correlation of fast and slow chemical shift spinning sideband patterns under fast magic-angle spinning, J. Magn. Reson. 160 (2003) 40–46.
[14] T. Gullion, Extended chemical-shift modulation, J. Magn. Reson. 85 (1989) 614–619.
[15] S. De Lacroix, J.J. Titman, A. Hagemeyer, H. Spiess, Increased resolution in MAS NMR spectra by two-dimensional separation of sidebands by order, J. Magn. Reson. 97 (1992) 435–443.
[16] R.M. Orr, M.J. Duer, S.E. Ashbrook, Correlating fast and slow chemical shift spinning sideband patterns in solid-state NMR, J. Magn. Reson. 174 (2005) 301–309.
[17] M. Strohmeier, D.M. Grant, A new sensitive isotropic–anisotropic separation experiment—SPEED MAS, J. Magn. Reson. 168 (2004) 296–307.
[18] A. Bax, N.M. Szeverenyi, G.E. Maciel, Chemical shift anisotropy in powdered solids studies by 2D FT CP/MAS NMR, J. Magn. Reson. 51 (1983) 400–408.
[19] J.Z. Hu, A.M. Orendt, D.W. Alderman, R.J. Pugmire, C.H. Ye, D.M. Grant, Measurement of ^{13}C chemical-shift tensor principal values with a magic-angle turning experiment, Solid State Nucl. Magn. Reson. 3 (1994) 181–197.
[20] J.Z. Hu, W. Wang, F. Liu, M.S. Solum, D.W. Alderman, R.J. Pugmire, D.M. Grant, Magic-angle-turning experiments for measuring chemical-shift-tensor principal values in powdered solids, J. Magn. Reson. 113 (1995) 210–222.

[21] R. Tycko, G. Dabbagh, P.A. Mirau, Determination of chemical-shift-anisotropy lineshapes in a two-dimensional magic-angle-spinning NMR experiment, J. Magn. Reson. 85 (1989) 265–274.
[22] Y. Yarim-Agaev, P.N. Tutunjian, J.S. Waugh, Sample spinning at the magic-angle with rotation-synchronized rf pulses, J. Magn. Reson. 47 (1982) 51–60.
[23] J.C.C. Chan, R. Tycko, Recoupling of chemical shift anisotropies in solid-state NMR under high-speed magic-angle spinning and in uniformly ^{13}C-labeled systems, J. Chem. Phys. 118 (2003) 8378–8389.
[24] Y. Ishii, T. Terao, Manipulation of nuclear spin hamiltonians by rf-field modulations and its applications to observation of powder patterns under magic-angle spinning, J. Chem. Phys. 109 (1998) 1366–1374.
[25] Z. Gan, High-resolution chemical shift and chemical shift anisotropy correlation in solids using slow magic angle spinning, J. Am. Chem. Soc. 114 (1992) 8307–8310.
[26] L. Frydman, G. Chingas, Y. Lee, P. Grandinetti, M. Eastman, G. Barrall, A. Pines, Variable-angle correlation spectroscopy in solid-state nuclear magnetic resonance, J. Chem. Phys. 97 (1992) 4800–4808.
[27] Y. Ishii, J. Ashida, T. Terao, ^{13}C–^{1}H dipolar recoupling dynamics in ^{13}C multiple-pulse solid-state NMR, Chem. Phys. Lett. 246 (1995) 439–445.
[28] R. Witter, S. Hesse, U. Sternberg, Powder pattern recoupling at 10 kHz spinning speed applied to cellulose, J. Magn. Reson. 161 (2003) 35–42.
[29] D.J. States, R.A. Haberkorn, D.J. Ruben, A two-dimensional nuclear Overhauser experiment with pure absorption phase in four quadrants, J. Magn. Reson. 48 (1982) 286–292.
[30] J. Keeler, D. Neuhaus, Comparison and evaluation of methods for two-dimensional NMR spectra with absorption mode lineshapes, J. Magn. Reson. 63 (1985) 454–472.
[31] M.M. Maricq, J. Waugh, NMR in rotating solids, J. Chem. Phys. 70 (1979) 3300–3316.
[32] M.H. Levitt, C.E. Hughes, P.K. Madhu, Cogwheel phase cycling, J. Magn. Reson. 155 (2002) 300–306.
[33] P. Bachmann, W.P. Aue, L. Müller, R.R. Ernst, Phase separation in two-dimensional spectroscopy, J. Magn. Reson. 28 (1977) 29–39.
[34] E. Hughes, T. Gullion, A simple, inexpensive and precise magic-angle spinning speed controller, Solid State Nucl. Magn. Reson. 26 (2004) 16–21.
[35] A.E. Bennett, C. Rienstra, M. Auger, K.V. Lakshmi, R. Griffin, Heteronuclear decoupling in rotating solids, J. Chem. Phys. 103 (1995) 6951–6958.
[36] T. Braunoger, P. Wormald, P. Hodgkinson, Improved proton decoupling in NMR spectroscopy of crystalline solids using the SPINAL-64 sequence, Monatsh. Chem. 133 (2002) 1549–1574.
[37] S. Hartmann, E. Hahn, Nuclear double resonance in the rotating frame, Phys. Rev. 128 (1962) 2042–2053.
[38] G. Metz, X. Wu, S. Smith, Ramped-amplitude cross-polarization in magic-angle-spinning NMR, J. Magn. Reson. Ser. A 110 (1994) 219–227.
[39] SciFace Software GmbH & Co. KG, Mupad Computer Algebra System, Paderborn.
[40] M. Bak, J. Rasmussen, N. Nielsen, SIMPSON: a general simulation program for solid-state NMR spectroscopy, J. Magn. Reson. 147 (2000) 296–330.
[41] T. Gullion, Measurement of dipolar interactions between spin-1/2 and quadrupolar nuclei by rotational-echo, adiabatic-passage double-resonance NMR, Chem. Phys. Lett. 246 (1995) 325–330.
[42] N. Ivchenko, C.E. Hughes, M.H. Levitt, Application of cogwheel phase cycling to sideband manipulation experiments in solid-state NMR, J. Magn. Reson. 164 (2003) 286–293.
[43] S. Pausak, J. Tegenfeldt, J.S. Waugh, ^{13}C chemical shielding tensors in polyalkylbenzenes, J. Chem. Phys. 61 (1974) 1338–1344.